IMOTHEP
GETTING HYBRID ELECTRIC

D4.9: FINAL BATTERY MODEL DOCUMENTATION

SECURITY: PUBLIC

Lead beneficiary: KIT

Contractual due date: June 2023

Actual submission date: 20 June 2023

Grant Agreement number:	875006
Project acronym:	IMOTHEP
Project title:	Investigation and Maturation of Technologies for Hybrid Electric Propulsion
Start date of the project:	01/01/2020
Duration:	48 months
Project coordinator:	Philippe NOVELLI (ONERA)
Phone:	+33 1 80 38 69 14
E-mail:	philippe.novelli@onera.fr
Project website address:	www.imothep-project.eu

This project has received funding from the European Union's Horizon 2020 research and innovation programme under grant agreement No 875006.

EXECUTIVE SUMMARY

This document summarises the three years activity of KIT of modelling solid-state batteries based on data exchange with AIT to investigate emerging all-solid-state battery technology appropriate for future aviation propulsion and power systems.

DOCUMENT INFORMATION

DOCUMENT NAME	W4.9 - Final battery model documentation
VERSION	6
VERSION DATE	20/06/2023
SECURITY	Public

DOCUMENT APPROVALS

	NAME	ORGANISATION	DATE
COORDINATOR	Ph. Novelli	ONERA	16/05/2023
WP LEADER	D Varchetta	GE Avio	18/03/2023
TASK LEADER	H. Kühnelt	AIT	24/03/2023
OTHER (QUALITY)	D. Behrendt	L-UP	30/05/2023

DOCUMENT HISTORY AND LIST OF AUTHORS

VERSION	DATE	MODIFICATION	NAME (ORGANISATION)
V1	28/02/2023	Creation	S. Toghyani (KIT)
V2	09/03/2023	Revision	D Varchetta (GE Avio)
V3	17/03/2023	Further complements	S. Toghyani (KIT)
V4	23/03/2023	Further complements	S. Toghyani (KIT)
V5	30/05/2023	Coordinator's and quality review	Ph. Novelli (ONERA), D. Behrendt (L-UP)
V6	20/06/2023	Complements further to coordinator's review	S. Toghyani (KIT)

DISTRIBUTION LIST

FULL NAME OR GROUP	ORGANISATION
Public	Not applicable

TABLE OF CONTENT

LIST OF FIGURES

LIST OF TABLES

Glossary

Acronym	Signification
ASSB	All-solid-state batteries
AIT	Austrian Institute of Technology
BHL	Bauhaus Luftfahrt
CB	Carbon black
DOD	Depth of discharge
GED	Gravimetric energy density
HFE	Hydrofluoroether
HCB	Highly concentrated electrolyte
IL	Ionic Liquid
KIT	Karlsruhe Institute of Technology
LATP	$Li_{1.3}Al_{0.3}Ti_{1.7}(PO_4)_3$
LLZTO	$Li_{6.4}La_3Zr_{1.4}Ta_{0.6}O_{12}$
LiTFSI	Lithium bis (fluorosulfonyl)imide
LIFSA	(fluorosulfonyl) lithium amide

LIB	Lithium-ion battery
LE	Liquid electrolyte
NASICON	Sodium (Na) super ionic conductor
NMC811	$LiNi_{0.8}Mn_{0.1}Co_{0.1}O_2$
NMC622	$LiNi_{0.6}Mn_{0.2}Co_{0.2}O_2$
OCV	Open circuit voltage
P2D	Pseudo-two-dimensional
PEO	Poly (ethylene oxide)
PIL	Polymerised ionic liquid
REG-CON	Regional-Conservative
SE	Solid electrolyte
SIC	Single-ion conductor
SL	sulfolane
SOC	State of charge
SPCE	Solid polymer composite electrolytes
tp	Lithium transfer number
VED	Volumetric energy densities

1. INTRODUCTION

This document summarises the three-year activity of KIT of modelling solid-state batteries based on data exchange with AIT to investigate emerging all-solid-state battery technology appropriate for future aviation propulsion and power systems.

2. BATTERIES

2.1. Model description

As the aircraft industry becomes more committed to sustainable aviation, hybrid-electric propulsion systems containing batteries with higher specific energy attract increasing attention to reduce fuel consumption. This approach is investigated in the context of the IMOTHEP (Investigation and Maturation of Technologies for Hybrid Electric Propulsion) European project, which seeks to identify promising hybrid aircraft configurations and study the associated technology bricks [1]. However, the main barrier to future progress in this kind of aircraft is the low specific energy of batteries. Additionally, to fulfil the requirements of high specific energy and power, capability to operate in a wide range of environmental conditions, and low depths of discharge, both the chemistry and package design of batteries for aircraft applications should be optimised. This brings additional challenges for the battery community [2]. The liquid electrolytes (LE), which are currently utilised in many lithium-ion batteries (LIB), exhibit high ionic conductivities and allow for faster interface kinetics. However, because of their high flammability, liquid electrolytes pose a safety issue [3]. Battery safety is more crucial than ever with the increased specific energy of LIB used to power electric vehicles and for long-range applications. This feature motivated the battery society to develop next-generation chemistries with non-flammable nature and long life, such as all-solid-state batteries (ASSB).

Solid electrolytes (SE), which are non-flammable in nature, could be a promising option for future aircraft. However, the batteries with such electrolytes have substantial reaction overpotentials and low capacity, consequently low specific energy at elevated current rates, [4]. This is because the kinetic properties of solid electrolytes employed in ASSB are constrained by their high interfacial resistance, and low ionic conductivity, especially at ambient temperature. Using hybrid battery cells is one way to improve ASSB performance.

Within IMOTHEP, the oxide-based solid-state batteries are investigated due to their relatively high ionic conductivity, ease of handling, and chemical stability in contact with Li metal and high cathode voltage materials [5]. The Austrian Institute of Technology (AIT) studied such technology at the coin cell level. Then, the experimental data of AIT are fed into the physics-based modelling of KIT (Karlsruhe Institute of Technology) to attain a deeper understanding of the behaviour of batteries and their integration into the electric powertrain.

As shown in Figure 1, the single cell of the battery is comprised of Li metal as the anode side, single ion conductor (SIC) electrolytes or solid polymer composite electrolytes (SPCE) as the solid separator, and the cathode, which is composed of NMC811 active material (80% of nickel, 10% of cobalt and 10% of manganese (8:1:1)) and solid electrolyte (SE).

The area of battery modelling is vast, with several available models for selection. These models differ in terms of complexity, reliability, and computational cost. The three most common battery models are data-driven models, equivalent circuit models, and mechanistic models. Mechanistic models are based on chemical and physical knowledge and aim to interpret the processes that take place within or between the components,

which affect the battery performance. The P2D model is the most common mechanistic model for single cells [6].

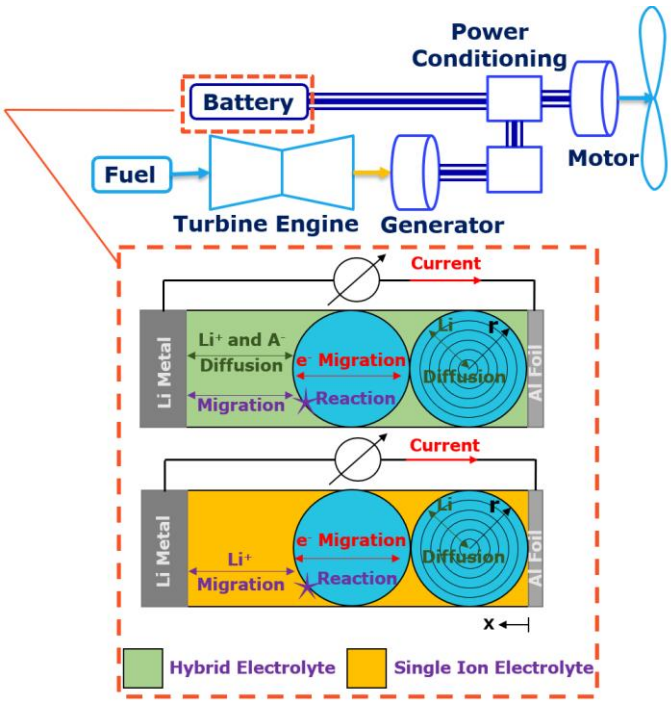

Figure 1: Hybrid-electric propulsion with solid-state batteries

KIT implemented a P2D model to simulate the electrochemical performance of Li-ASSB with SIC and SPCE electrolytes. This model considers diffusion, lithium-ion accumulation as well as electrical charge in the direction of electrode thickness, diffusion, and lithium-ion accumulation in a radial dimension, and electrochemical reactions at electrodes [7]. The block diagram of the P2D model is depicted in Figure 2.

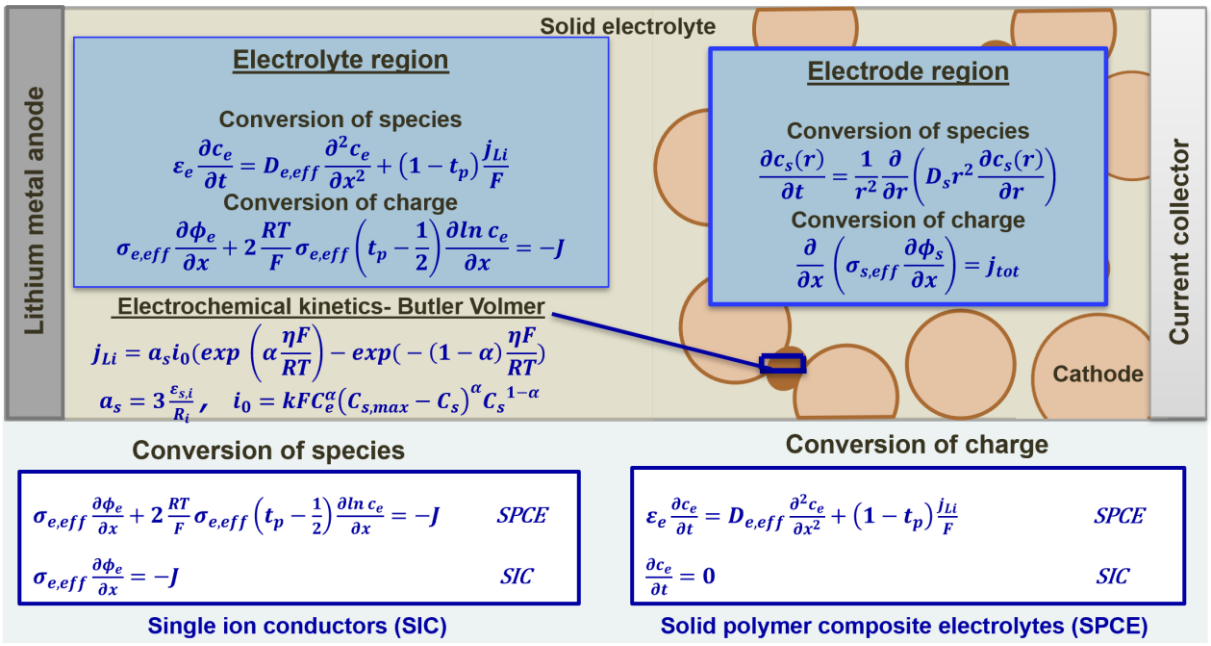

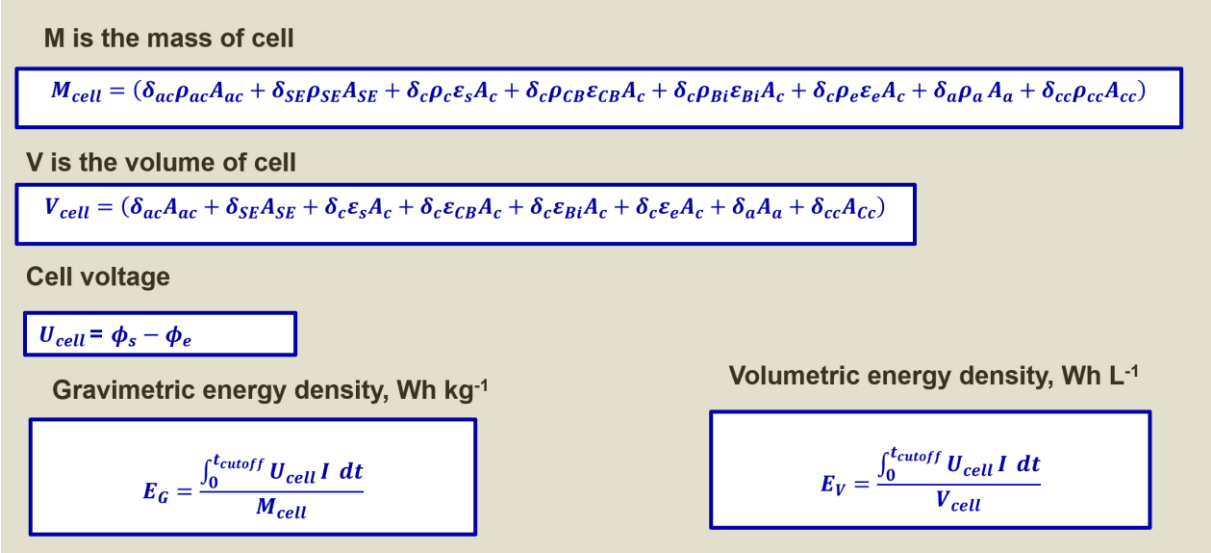

Figure 2: Block diagram of P2D electrochemical model

where c_e is Li-ion concentration in electrolyte, ε_e is the volume fraction of electrolyte, j_{Li} is the intercalation current density, t_p is Li transfer number, F is Faraday constant, D_e is electrolyte diffusion coefficient, φ_e is electrolyte potential, σ_e is electrolyte phase ionic conductivity, R is the universal gas constant, T is temperature, c_s is the Li concentration in the active material, φ_s is solid phase potential, σ_s is electronic conductivity of NMC, D_s is Li diffusivity in the active material, a_s is the volume-specific active area, η is the electrochemical overpotential, k is the reaction rate constant, α is charge transfer coefficient, c_{max} is the maximal Li concentration in the active material, ε_s is the volume fraction of active material, and R in the equation of the volume-specific active area is Particle size.

In the end, cell voltage, the gravimetric energy density, E_G, can be computed by dividing the integral of instantaneous power from 0 to time to reach the cut-off voltage ($t_{cut-off}$) by the mass of the cell, M_{cell}. For estimating the mass of the cell, M_{cell}, the mass of the current collectors, anode and cathode electrodes, solid electrolytes, and non-active components, i.e., carbon black (CB), and binder are considered. The volumetric energy density, E_V, is also estimated by dividing cell energy by the volume of the cell, V_{cell}.

A_{ac}, A_{cc}, A_{SE}, A_a, and A_c are the geometrical area of the anode and cathode current collectors, solid electrolyte, and the anode and cathode electrodes, respectively. δ_a, δ_c, δ_{SE}, δ_{ac}, and δ_{cc} are thicknesses of the anode, cathode, solid separator, anode current collector and cathode current collector, respectively. ε_{CB} and ε_{Bi} are the volume fraction of CB and binder. It should be noted that for comparative analysis of a wide range of electrolytes, KIT exclusively used typical electrolyte parameters from literature, e.g. the thickness, ionic conductivity, and tp of a given hybrid electrolyte, as shown in Table 1.

Table 1: Li-ion transfer number, ionic conductivity, and thickness of hybrid solid electrolytes

Parameters	Group type	tp	Ionic conductivity, S cm^{-1}	Thickness of SE layer, μm
PEO-LiTFSI [8]	*Polymer*	*0.15*	2.65×10^{-4}	*130-150*
PEO-PPC- LiTFSI [9]	*Polymer*	*0.177*	2.71×10^{-4}	*130-150*
PEO-PPC- LiTFSI/LLTO (8 wt%) [9]	*SPCE based on perovskite*	*0.227*	4.72×10^{-4}	*135*
PEO- LiTFSI/LLTO (5 wt%) [8]	*SPCE based on perovskite*	*0.195*	3.63×10^{-4}	*135*
PEO- LiTFSI /LLZTO (5.2 vol%) [10]	*SPCE based on garnet*	*0.31*	2.31×10^{-4}	*40*
PEO- LiTFSI /LLZTO (8.6 vol%) [10]	*SPCE based on garnet*	*0.37*	3.05×10^{-4}	*40*
PEO- LiTFSI /LLZTO (10.5 vol%) [10]	*SPCE based on garnet*	*0.42*	4.65×10^{-4}	*40*
PEO- LiTFSI /LLZTO (12.7 vol%) [10]	*SPCE based on garnet*	*0.46*	5.63×10^{-4}	*40*
PEO- LiTFSI /LLZTO (15.1 vol%) [10]	*SPCE based on garnet*	*0.43*	5.07×10^{-4}	*40*
PEO- LiTFSI /LLZTO (17.9 vol%) [10]	*SPCE based on garnet*	*0.39*	4.72×10^{-4}	*40*
PEO- LiTFSI /LLZTO (21.1 vol%) [10]	*SPCE based on garnet*	*0.33*	3.68×10^{-4}	*40*
PIL-LiTFSI [11]	*Polymer*	*0.07*	4.84×10^{-4}	*200*
PIL-LiTFSI/LATP (10 wt%) [11]	*SPCE based on NASICON*	*0.21*	5.92×10^{-4}	*200*
PIL-LiTFSI/LATP (20 wt%) [11]	*SPCE based on NASICON*	*0.15*	4.09×10^{-4}	*200*
PIL-LiTFSI/LATP (30 wt%) [11]	*SPCE based on NASICON*	*0.12*	3.5×10^{-4}	*200*
PIL-LiTFSI/LATP (40 wt%) [11]	*SPCE based on NASICON*	*0.09*	3.06×10^{-4}	*200*
PEO- LiTFSI/LAGP (20 wt%) [12]	*SPCE based on NASICON*	*0.168*	2.94×10^{-4}	*200*
PEO- LiTFSI/LAGP (40 wt%) [12]	*SPCE based on NASICON*	*0.175*	5.17×10^{-4}	*200*
PEO- LiTFSI/LAGP (60 wt%) [12]	*SPCE based on NASICON*	*0.213*	5.8×10^{-4}	*200*
LLZO [13]	*SIC based on garnet*	*1*	8.41×10^{-3}	*300*
LLZTO [13]	*SIC based on garnet*	*1*	9.54×10^{-3}	*300*
LLTO [14]	*SIC based on perovskite*	*1*	5.27×10^{-3}	*300*
LATP [15–17]	*SIC based on NASICON*	*1*	5×10^{-3}	*300*

MATLAB 2021b is adopted to implement all simulations for the ASSB model. The finite volume method is applied for spatial discretisation of partial differential equations, and the ODE15 solver solves the time derivatives. The geometrical features of the battery, along with physical and electrochemical properties, are given in Table 2, which is based on experimental data from AIT and available literature data.

Table 2: Geometry data and physical and electrochemical features of the single cell

Geometry data			
Parameters	***Symbol***	***Ref***	***Value***
Thickness of anode/cathode, µm	δ_a/δ_c	*Delivered data from AIT*	*70/55*
Thickness of separator	δ_{SE}	[8–18]	*Table 1*
Thickness of anode/cathode current collector, µm	δ_{ac}/δ_{cc}	*Delivered data from AIT*	*0/15*
Diameter of anode/cathode/solid electrolyte, cm	$D_a/D_c/D_{SE}$	*Delivered data from AIT*	*1.6/1.5/1.9*
Geometry of pouch cell		*Delivered data from AIT*	*Anode: 10.0cmx7.0cm Cathode: 9.9cmx6.9cm Electrolyte: 10.1cmx7.1cm*
Volume fraction of active material	ε_s	*Delivered data from AIT*	*0.44*
Particle size, µm	R	*Delivered data from AIT*	*NMC622: D10(µm): 5.54 D50(µm): 10.10 D90(µm): 16.29 NMC811: D10(µm): 5.46 D50(µm): 10.31 D90(µm): 17.07*
Physical and electrochemical properties			
Temperature, °C	*T*	*Delivered data from AIT*	*60*
Lithium transfer number	*tp*	[8–18]	*Table 1*
Density of NMC811/, kg m^{-3}	ρ_c	*Delivered data from AIT*	*4800*
Density of Li, kg m^{-3}	ρ_a	*Delivered data from AIT*	*534*
Density of Al, kg m^{-3}	ρ_{cc}	*Delivered data from AIT*	*2700*
Electronic conductivity of NMC, S m^{-1}	σ_s	[19]	*0.17*
Electrolyte phase ionic conductivity, S m^{-1}	σ_e	[8–18]	*Table 1*
Li diffusivity in active material, m^2 s^{-1}	D_s	*Delivered data from AIT*	*4.84E-14*
Electrolyte diffusion coefficient, m^2 s^{-1}	D_e	*Literature*	*Based on Einstein relation*
Maximum solid phase concentration, mol m^{-3}	$c_{s,max}$	[19]	*50060*
Initial electrolyte concentration, mol m^{-3}	$c_{e,0}$	[20]	*1200*
Charge transfer coefficient	α	*Literature*	*0.5*
Open circuit voltage, V	U_0	*Delivered data from AIT*	*Table 1*
Double-layer capacitance at cathode/electrolyte interface, Fm^{-2}	C_{DL}	[21]	*0.2*

For a starting point for all the simulations, the Open Circuit Voltage (OCV) curve is required that is adjusted based on AIT measurement. They made two types of cells for the OCV measurement: a rectangular shape for pouch cell application with NMC622 (60% of nickel, 20% of cobalt and 20% of manganese (6:2:2)) as the cathode, and a circular shape for coin cell with NMC811. Based on experimental data that is delivered by AIT, KIT derived the OCV equations for these two different cathode materials using curve fitting, as described in Table 3. These equations are then implemented into the P2D model for the modelling of ASSB.

Table 3: OCV equations for the NMC811 and NMC622 based on AIT measurement

U0 for NMC811		
$\tilde{c}_s = \frac{c_s}{c_{s,max}}$		
$a_1 = 5.878e{+}10$ $b_1 = -8.039$ $c_1 = 1.634$ $a_2 = 2.176$ $b_2 = 0.1096$ $c_2 = 0.3259$ $a_3 = 3.195$ $b_3 = 0.6032$ $c_3 = 0.433$		$a_4 = 0.9865$ $b_4 = 0.8959$ $c_4 = 0.2024$ $a_5 = 0.5468$ $b_5 = 0.9607$ $c_5 = 0.1073$ $a_6 = 0.3946$ $b_6 = 0.997$ $c_6 = 0.05753$
$U = a_1 exp\left(-\left(\frac{\tilde{c}_s - b_1}{c_1}\right)^2\right) + a_2 exp\left(-\left(\frac{\tilde{c}_s - b_2}{c_2}\right)^2\right) + a_3 exp\left(-\left(\frac{\tilde{c}_s - b_3}{c_3}\right)^2\right) + a_4 exp\left(-\left(\frac{\tilde{c}_s - b_4}{c_4}\right)^2\right) + a_5 exp\left(-\left(\frac{\tilde{c}_s - b_5}{c_5}\right)^2\right) + a_6 exp\left(-\left(\frac{\tilde{c}_s - b_6}{c_6}\right)^2\right)$		
U0 for NMC622		
$a_1 = 7.066$ $b_1 = -1.479$ $c_1 = 1.871$ $a_2 = 1.725$ $b_2 = 0.877$ $c_2 = 0.6847$ $a_3 = 0.1751$ $b_3 = 0.9245$ $c_3 = 0.1443$		
$U = a_1 exp\left(-\left(\frac{\tilde{c}_s - b_1}{c_1}\right)^2\right) + a_2 exp\left(-\left(\frac{\tilde{c}_s - b_2}{c_2}\right)^2\right) + a_3 exp\left(-\left(\frac{\tilde{c}_s - b_3}{c_3}\right)^2\right)$		

2.2. Verification of battery model based on AIT measurement

KIT implemented experimental data of AIT into the numerical model for the validation of the simulation. Identical operating and geometrical conditions are performed for comparison. The considered pouch cell consists of NMC as the cathode, and a mix of NASICON electrolyte (LATP) and PEO with LiTFSI as the electrolyte. They simulated the discharge voltage of the cell against the specific capacity at different current rates and compared the results with experimental data from AIT. As shown in Figure 3, the numerical results are in good agreement with the experimental measurements for various current rates.

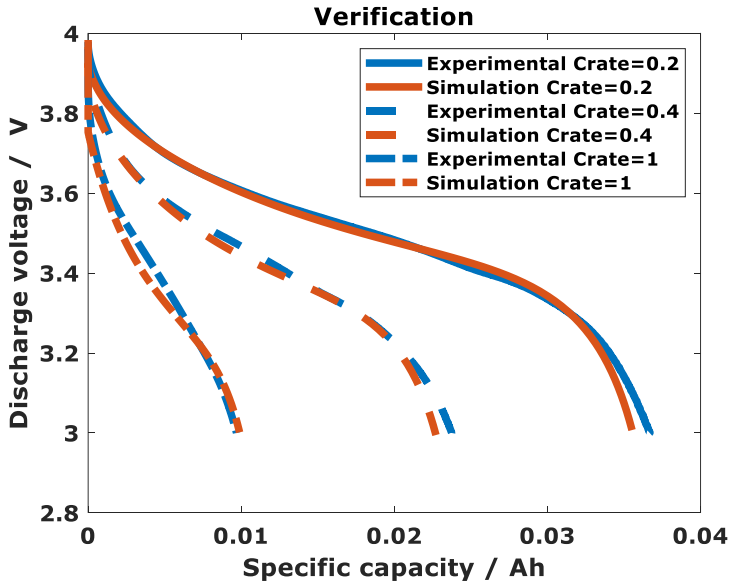

Figure 3: Verification of battery model based on AIT measurement [4]

2.3. A COMPARATIVE STUDY OF VARIOUS SIC AND HYBRID ELECTROLYTES OF OXIDE AND POLYMER

In this section, the performance of several types of SPCE electrolytes with different percentages of inorganic oxides-based electrolytes is first examined. As not every electrolyte can presently be manufactured in thin layers, experimentally reported thicknesses of solid electrolytes for each group of electrolytes are considered, as detailed in Table 1. The best-performing electrolytes among various groups of oxide electrolytes, i.e., perovskite, garnet, and NASICON, and hybrid electrolytes are then identified. Furthermore, compatibility with Li and the high-voltage cathode should be taken into account when choosing the best electrolyte type; the selected electrolyte should be stable up to 4.5 V because the operating window of NMC811 is up to 4.5 V [22].

Figure 5-a and *Figure 5*-b show a performance comparison of oxide-based SPCE electrolytes in terms of Gravimetric Energy Density (GED) at two discharge rates. It is assumed that all cells have the same anode and cathode electrodes. The only difference between cells is the electrolyte type, separator thickness (which has been empirically demonstrated in the literature due to production restrictions), ionic conductivity, density, and tp (as described in Figure 4 and tp of a given hybrid electrolyte, as shown in Table 1). All these simulations show that, at low discharge rates, density is the most critical factor affecting GED. However, at an elevated discharge rate, besides density also transport relevant parameters, i.e. ionic conductivity, and tp play a significant role for the GED. Since we aim to find the optimal design of the electrode for high-energy applications as well as for high power and high energy application simultaneously, the best hybrid electrolyte should not have mass transfer limitations at elevated discharge rates. For this reason, we selected the best electrolyte for each group, marked in red based on the results of *Figure 5*-b.

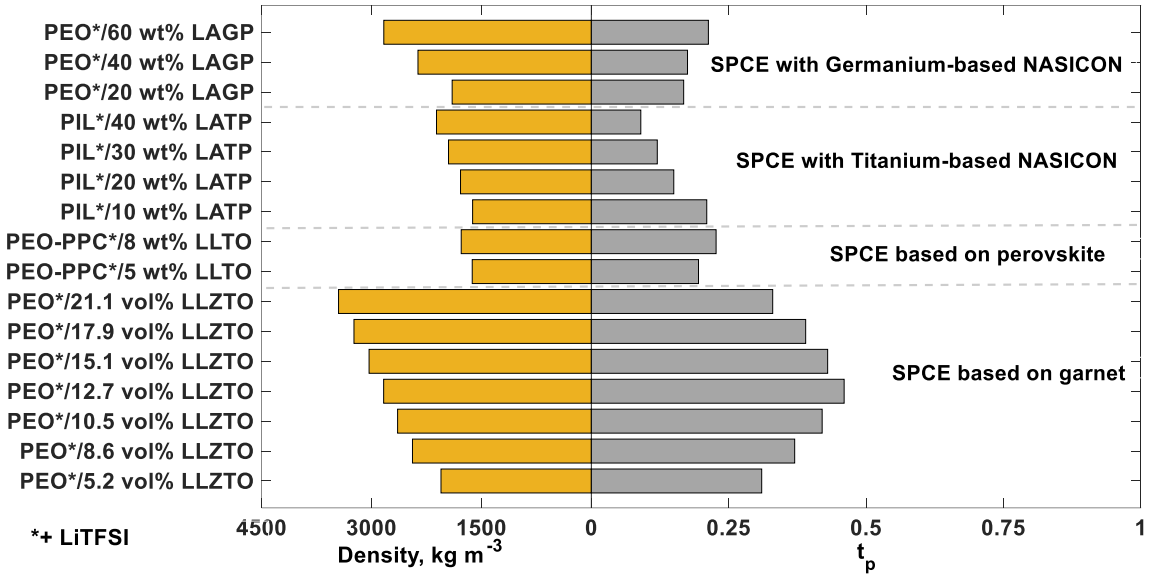

Figure 4: Lithium transfer number (tp) and density of SPCE electrolytes [4]

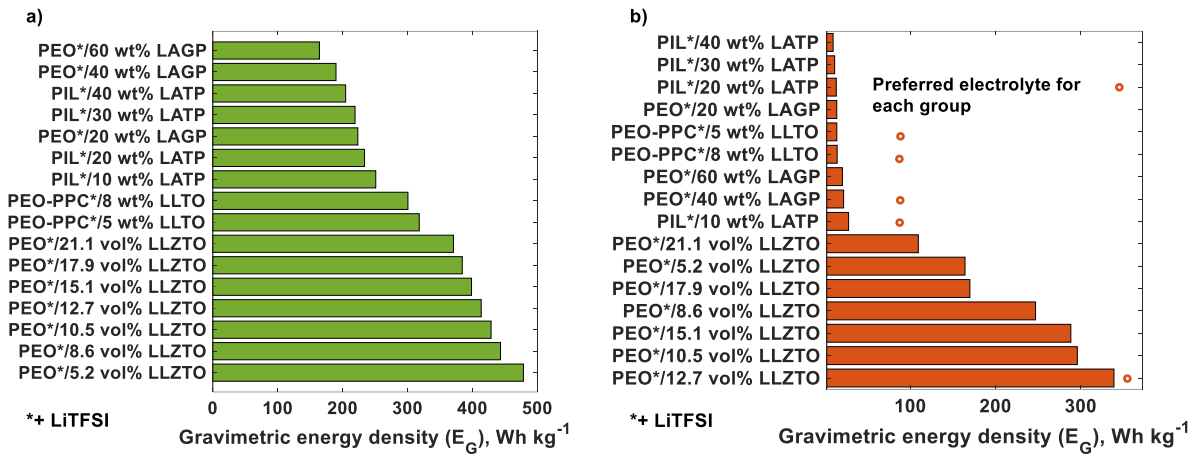

Figure 5: Impact of various compositions of SPCE electrolytes at 60 °C on the GED for a cell with Li metal as the anode, and NMC811 as cathode at a) 0.1C, b) 1C [4]

We then compared SIC electrolytes, polymer electrolytes, and the identified best hybrid electrolyte, to select the most suitable solid electrolyte in terms of gravimetric and volumetric energy densities. In the first comparison, we consider the reported thickness of solid electrolytes, which is based on the current technology of solid-state batteries, as mentioned in Table 1. In the second comparison, the modelling is performed with the same thickness of 40 µm for all solid electrolytes to answer the following question: Which kind of solid electrolyte is the most promising for the energy demand in the aviation context if the thickness can be reduced in the manufacturing step to the current thickness of garnet-based hybrid electrolytes?

Figure 6-a shows the model-predicted gravimetric and volumetric energy densities (VED) of the cells with various solid electrolyte types and their reported thickness. As shown in the figure, there is no considerable discrepancy in the GED of SIC based on LLZO, LLTO, and LLZTO at a low and elevated discharge rate. LLZTO has the highest ion conductivity among the chosen SIC electrolytes. Owing to its high density, LLZTO does not have the highest GED. The highest gravimetric energy density among SIC electrolytes is observed for LATP ones at 0.1C. However, it shows low gravimetric and volumetric energy densities due to its large separation layer. Due to the Li dendrite growth issue in these types of batteries and the necessity to avoid internal short circuits, a thick separator layer of ca. 300 µm should be employed in the construction of Li-ASSB-based on SIC electrolyte. With such high thicknesses and densities, it is impossible to attain attractive GED with SIC electrolytes. A hybrid electrolyte of oxide and polymer could be a promising solution to enhance the gravimetric and volumetric energy densities of Li-based ASSB [8–12].

The SPCE with 12.7 vol% of LLZTO has the maximum GED in comparison with other hybrids, SIC, and polymer electrolytes. The explanation for this is that SPCE with LLZTO can be manufactured much thinner so that less ionic overpotential is expected. They are additionally advantageous because they are more stable in contact with a lithium metal anode, and the electrochemical window of PEO-LiTFSI/LLZTO (12.7 vol%) is more than 4.7 V. Hence, PEO-LiTFSI/LLZTO (12.7 vol%) could be an appropriate option to achieve a higher GED in coupling with Li and high voltage cathode materials. However, the amount of its gravimetric and volumetric energy densities is not high enough for aviation applications.

Figure 6-b shows which electrolyte is the most promising in terms of high energy-density batteries if the thickness of all electrolytes is reduced to the same level as garnet-based hybrid electrolytes (40 µm). According to the conducted simulations, the maximum GED of 525 Wh kg^{-1} at 0.1C is observed for SPCE with 10 wt% of LATP. Thus, this type of solid electrolyte could be a promising choice for future aircraft.

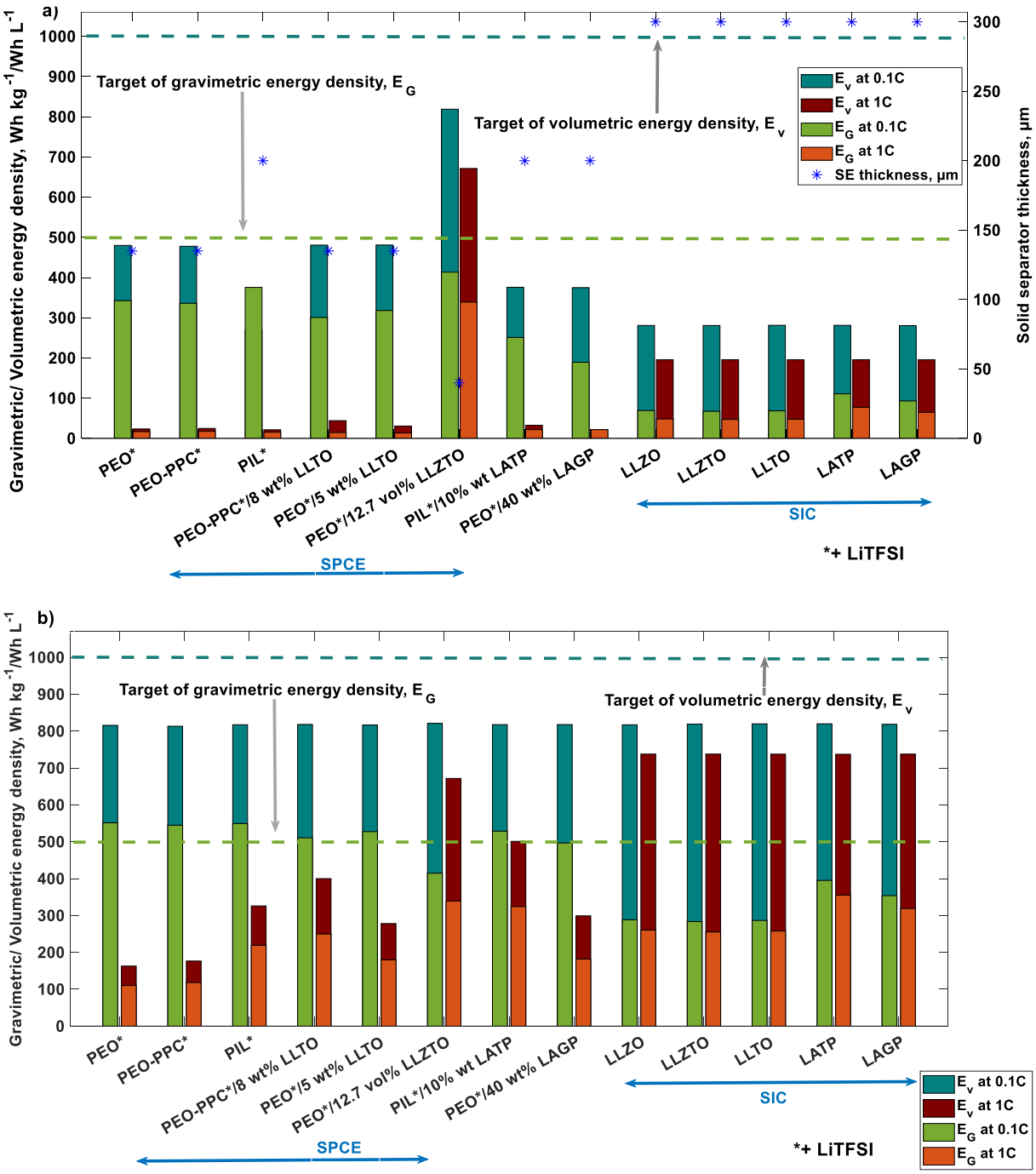

Figure 6: Comparison of SIC electrolyte and SPCE in terms of gravimetric and volumetric energy densities for a cell with Li metal as the anode, and NMC811 as cathode at a) actual SE thickness, b) SE thickness of 40 µm for different discharge rates

In reality, due to battery management systems, contacting technology, sensors, and other factors, it is impossible to obtain the same energy density at the cell and system levels. As a result, energy density decreases from cell levels to higher levels. For this purpose, the efficiency rate can be defined as below:

$$\text{Efficiency rate} = \frac{Energy\ density\ of\ higher\ level\ (exp.: system)}{Energy\ density\ of\ lower\ level\ (exp.: cell)} \quad (1)$$

The efficiency rate of the battery from cell level to pack level is considered equal to 0.742, which is used for the prismatic and pouch cells [23]. In Table 4, we summarised the *GED for the best solid electrolytes based on the current technology and promising ones for the future.*

Table 4: GED of identified best hybrid electrolyte-based current technology of SE and the most promising ones for the future at 0.1C and 1C

0.1C			
	Anode	**Cathode**	**GED (cell level)**
Based current technology	*Li*	*NMC811 & LLZTO-HSE*	*411*
Promising SE for future		*NMC811 & LATP-HSE*	*525*
1C			
	Anode	**Cathode**	**GED (cell level)**
Based current technology	*Li*	*NMC811 & LLZTO-HSE*	*342*
Promising SE for future		*NMC811 & LATP-HSE*	*324*

As shown in Table 4, based on the current technology of the solid electrolyte, the GED of the ASSB is still low, particularly at elevated discharge rates. One way to improve the GED of the ASSB is to optimise the design parameters of the battery. Because we aim to optimise the cell using components that are already manufacturable, a hybrid electrolyte with 12.7 vol% LLZTO, which can already now be produced in thin layers, is employed as the solid electrolyte. Therefore, in the next part, we will first perform the sensitivity analysis on the battery cell to determine which battery parameters drive the GED and then select decision variables for the optimisation of ASSB.

2.4. SENSITIVITY ANALYSIS

In order to estimate the sensitivity indices, KIT applied the variance-based global sensitivity approach, also known as the Sobol approach, which already proved suitable for analysing Li-ion batteries [20]. This approach is based on the decomposition of the variance of the model output into the summand of variance of individual or interaction of input parameters. The Sobol sensitivity indices estimate how much each input factor contributes to the variation of the model output. When a parameter has a low sensitivity index, this results in small changes in the final model output. If a parameter has a high sensitivity index, changing it causes the model output to change drastically [24].

$$V(Y) = \sum_{i=1}^{n} V_i + \sum_{i \le j \le n}^{n} V_{ij} + \cdots + V_{i,\ldots,n} \tag{2}$$

The first-order Sobol index, which represents the influence of a single input parameter on the model output, can be determined as the ratio of partial variance to the total variance. In contrast, the higher order of the Sobol index indicates the impact of input parameter interaction on the output results.

$S_i = \frac{V_i}{V}$ First-order Sobol index (3)

$S_{ij} = \frac{V_{ij}}{V}$ Second-order Sobol index (4)

The total sensitivity index or total effect of each input parameter can be defined as a sum of all orders of sensitivity index as follow [25]:

$$S_T = S_i + \sum_{i \neq j} S_{ij} + \cdots \quad (5)$$

As listed in Table 5, the chosen input parameters of the sensitivity analysis are Li transfer number, the thickness of cathode and electrolyte, particle size of cathode material, volume fraction of cathode material, the electric conductivity of solid phase, and tortuosity.

Table 5: List of input parameters for the sensitivity analysis of ASSB

Battery variables			
Variable name	***Minimum***	***maximum***	***Distribution type***
Lithium transfer number, t_p	*0.15*	*0.46*	*Uniform*
Cathode thickness, δ_C (µm)	*40*	*80*	*Uniform*
Solid electrolyte thickness, δ_{SE} (µm)	*40*	*100*	*Uniform*
Cathode particle radius, R_C (µm)	*3*	*13*	*Uniform*
Volume fraction of active material, ε_C	*0.4*	*0.65*	*Uniform*
Electric conductivity, σ_s (Sm^{-1})	*0.01*	*1*	*Uniform*
	Expected value	***Standard deviation***	***Distribution type***
Bruggeman factor, ß	*1.5*	*10%*	*Gaussian*

As demonstrated in Figure 7, the GED exhibits high sensitivities for the cathode and solid electrolyte thicknesses and the volume fraction of active materials in both discharge rates. Particle size and electrical conductivity are not sensitive, especially at a low discharge rate. tp and tortuosity, have a considerable influence on the battery performance at elevated discharge rates, due to transport limitations. Since the last two parameters are material-dependent or hard to control, and the aim was to optimise the cell without modifying material characteristics, they are not considered as decision variables for the optimisation model.

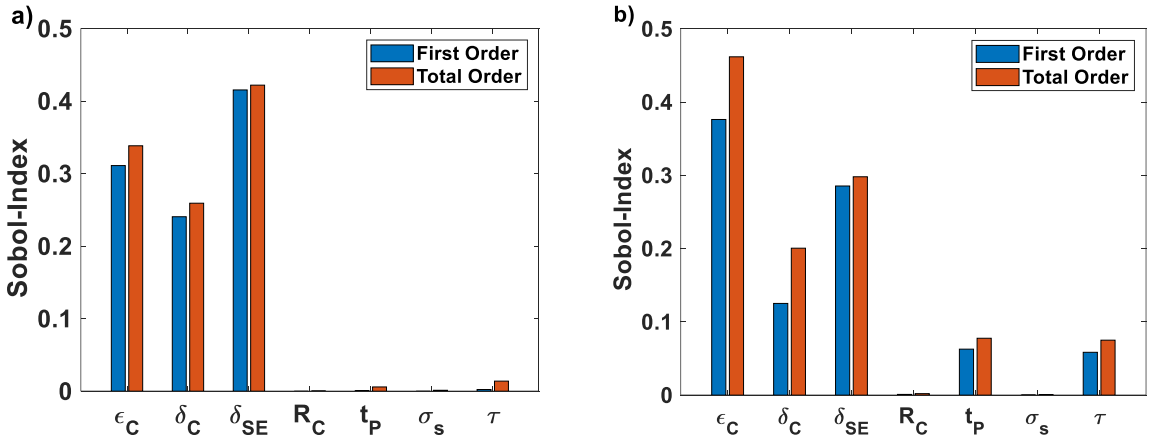

Figure 7: Comparison of the Sobol index of simulation with parameter variations for a cell with 12.7 vol% LLZTO, Li metal as the anode, and NMC811 as cathode at a) C-rate of 0.1, b) C-rate of 1 [4]

2.5. OPTIMISATION

Various mathematical methodologies have been used to deal with optimisation problems, such as classical methods and evolutionary algorithms. A classical approach like gradient-based methods is known to generate outstanding results in a short time, but they are prone to be stuck in a local optimum point. The classical approach does not function well over a wide diversity of problem domains, and they are inefficient when the search space is too broad [26]. To avoid the probability of being stuck at a local optimum point, here we applied the global optimisation algorithm for finding the optimum electrode design of the ASSB.

As demonstrated earlier, the hybrid electrolyte with 12.7 vol% of LLZTO has the best discharge battery performance, when taking into account present manufacturing constraints. Hence, we performed optimisation on the reference cell with this electrolyte including its typical thickness, ionic conductivity, tp, which are based on the experiments extracted from literature, to identify those cathode parameter values, i.e., cathode thickness and volume fraction of active material, which lead to the highest GED for a given C-rate. Since we aim to find the optimal design of the electrode for high-energy applications as well as for high-power and high-energy applications simultaneously, we did optimisation for two different discharge rates. We also performed simulations for the optimal design of cells for 0.1C and 1C at discharge rates of 1C and 0.1C, respectively to elucidate whether the optimal proposed design for a particular application at the respective C-rate is better than the reference.

As shown in Table 6, the cell with the optimal design for 0.1C shows the highest performance in terms of GED in comparison to the reference cell and optimised cell for 1C, discharged at 0.1C. The cell with the optimal design for 0.1C has a significantly thicker NMC electrode and a higher volume fraction of active material (63%) than the reference cell and the optimised cell for 1C. The optimised cell for 1C, discharged at 0.1C, performs worse than the reference cell at 0.1C, since the cathode thickness is thinner, resulting in lower theoretical capacity. Furthermore, this cell has a GED of 74 Wh kg^{-1}, which is significantly smaller than the optimised cell for 1C (351 Wh kg^{-1}) and thus cannot be used for high-power, high-energy applications.

Table 6: Comparison of reference and optimum solid-state battery design for a cell with 12.7 vol% LLZTO, Li metal as the anode, and NMC811 as cathode at two discharge rates

	δ_c (µm)	ε_s	VED, Wh L^{-1}	GED, Wh kg^{-1}
Reference design, 0.1C	*55*	*0.44*	*813*	*411*
Optimal design for 0.1C	*77*	*0.63*	*1251*	*618*
Optimised cell for 0.1C, discharge at 1C	*77*	*0.63*	*149*	*74*
	δ_{cat} (µm)	ε_s	VED, Wh L^{-1}	GED, Wh kg^{-1}
Reference design 1C	*55*	*0.44*	*677*	*342*
Optimal design for 1C	*43*	*0.48*	*722*	*351*
Optimised cell for 1C, discharge at 0.1C	*43*	*0.48*	*812*	*395*

0.1C → High energy application
1C → Energy-power-balanced application

In summary, the optimal designs strongly depend on the concrete objective, i.e., the optimal proposed design for a particular application does not perform well for all

applications. Furthermore, the GED at a relatively high C-rate of 1C is still not high enough. Therefore, in the following part, we look at potential solutions to improve the battery performance at elevated discharge rates.

3. POTENTIAL SOLUTIONS TO IMPROVE THE PERFORMANCE OF ASSB

3.1. USING HIGHLY CONCENTRATED LIQUID OR IONIC ELECTROLYTE IN THE CATHODE (CATHODIC ELECTROLYTE)

As mentioned earlier, the optimal energy-power-balanced cell shows a maximal GED of 351 Wh kg^{-1} at the cell level and 260 Wh kg^{-1} at the pack level considering an efficiency rate of 0.742 from cell level to pack level, which is not high enough for aviation application. The low GED could be due to the low ionic conductivity of SE, since the kinetic properties of solid-state electrolytes employed in all-solid-state lithium metal batteries are constrained by their high interfacial resistance, and low ionic conductivity, especially at ambient temperature. One solution to improve the SSB performance is to use hybrid battery cells combining liquid electrolytes with inorganic Solid Electrolyte (SE) separators or different SEs and polymer electrolytes, respectively.

The liquid electrolytes (LEs), which are currently utilised in many lithium-ion batteries, exhibit high ionic conductivities and allow for faster interface kinetics. However, because of their high flammability, LEs pose a safety issue. Battery safety is more crucial than ever with the increased energy density of lithium-ion batteries used to power electric vehicles and for long-range applications. This feature motivated the battery community to develop a non-flammable liquid electrolyte that eliminates the risk of battery fire and explosion, which is urgently required [27].

Due to the higher safety of highly concentrated LEs or ionic liquid electrolytes (ILs), they have been drawing increasing attention for use as the solvent in lithium batteries. Due to the higher oxidation stability of the ILs and the significantly reduced amount of free carbonate solvent in the highly concentrated electrolytes, increasing the salt concentration and adding the IL can significantly enhance the electrochemical stability window [28]. However, due to the high viscosity and low ionic conductivity of ILs in comparison to commonly utilised organic carbonate solvents, most lithium batteries using ILs have poor rate capability [3]. Introduction of diluent solvents into ILs like hydrofluoroether (HFE), which is a suitable diluent for high-concentration electrolytes because of its low viscosity and nonflammability, could reduce the viscosity of the pure ILs. HFE could also reduce the cost of ILs while also enhancing the ionic conductivity of ILs and their wetting capabilities for the separator surface [29].

For this project, we did a comprehensive literature study on different highly concentrated liquid or ionic electrolytes to identify the most suitable ones for energy-power-balanced applications. We applied electrolyte characteristics for the modelling, such as the lithium transfer number, ionic conductivity, and electrolyte diffusion coefficient based on available experimental data in the literature. Since hybrid SE performs well at a temperature of 60°C as we noted in ref. [4], we used the Arrhenius relation to take into account the dependence of electrolyte properties on temperature for those parameters which are not given at this temperature [30]. The electrochemical features of various cathodic electrolytes are given in Table 7.

Table 7: Electrochemical features of various cathodic electrolytes

Geometry data		
Parameters	***Symbol***	***Value***
Li-ion transfer number of LiFSI/IL-HFE [31]	*tp*	*0.495*
Diffusion coefficient Li-ion in the LiFSI/IL-HFE, m^2 s^{-1} [31]	D_e	4.9×10^{-11}
Ionic conductivity of LiFSI/IL-HFE, S cm^{-1}[31]	σ_e	8.1×10^{-3}
Li-ion transfer number of LiTFSI-([C4mim] [BF4] [32]	*tp*	*0.444*
Diffusion coefficient Li-ion in the LiTFSI-([C4mim] [BF4], m^2 s^{-1}[32]	D_e	1.99×10^{-11}
Ionic conductivity of LiTFSI-([C4mim] [BF4], S cm^{-1} [32]	σ_e	*0.143*
Li-ion transfer number of LiTFSI-([C4mim] [TFSI] [32]	*tp*	*0.445*
Diffusion coefficient Li-ion in the LiTFSI-([C4mim] [TFSI], m^2 s^{-1}[32]	D_e	1.8×10^{-11}
Ionic conductivity of LiTFSI-([C4mim] [TFSI], S cm^{-1} [32]	σ_e	*0.141*
Li-ion transfer number of LiBF4-sulfolane (SL) [33]	*tp*	*0.534*
Diffusion coefficient Li-ion in the LiBF4-sulfolane (SL), m^2 s^{-1} [33]	D_e	2.9×10^{-11}
Ionic conductivity of LiBF4-sulfolane (SL), S cm^{-1}[33]	σ_e	3.1×10^{-3}
Li-ion transfer number of LiFSA-sulfolane (SL) [33]	*tp*	*0.545*
Diffusion coefficient Li-ion in the LiFSA-sulfolane (SL), m^2 s^{-1} [33]	D_e	4.65×10^{-11}
Ionic conductivity of LiFSA-sulfolane (SL), S cm^{-1} [33]	σ_e	6.95×10^{-3}
Li-ion transfer number of LiTFSI + Pyr1,3FSI + H2 [34]	*tp*	*0.426*
Diffusion coefficient Li-ion in the LiTFSI + Pyr1,3FSI + H2, m^2 s^{-1} [34]	D_e	2.6×10^{-11}
Ionic conductivity of LiTFSI + Pyr1,3FSI + H2, S cm^{-1} [34]	σ_e	3.3×10^{-3}
Li-ion transfer number of PEC+LiFSI+Tio2 [35]	*tp*	*0.76*
Diffusion coefficient Li-ion in the PEC+LiFSI+Tio2, m^2 s^{-1} [35]	D_e	1.4×10^{-11}
Ionic conductivity of PEC+LiFSI+Tio2, S cm^{-1} [35]	σ_e	3.9×10^{-4}

As shown in Figure 8, two prospective highly concentrated electrolytes (HCE), LiFSA-sulfolane (SL) and LiFSI-IL-HFE, exhibit superior performance to the others. They provide relatively high specific energy even at a high C-rate, making them a suitable candidate for use in applications requiring an energy-power balance. The non-flammable highly concentrated electrolyte of LiFSA- SL, which is stable in contact with high cathode voltage materials, shows better performance than other highly concentrated electrolytes. Therefore, it could be one of the potential cathodic electrolyte choices; nonetheless, its cycling number is less than that of the other ones, i.e, LiFSI-IL-HFE as a cathodic electrolyte. Additionally, the highly concentrated electrolyte of LiFSI-IL-HFE is non-flammable and has high electrochemical stability in contact with high cathode voltage materials like NMC811 and a relatively high cycling number of 800. This electrolyte, in second place after LiFSI-IL-HFE, shows a good performance than other cathodic electrolytes. Therefore, due to its outstanding properties, this type of electrolyte was selected as a promising-identified electrolyte inside the cathode to improve the performance of ASSB, as stated in Table 8.

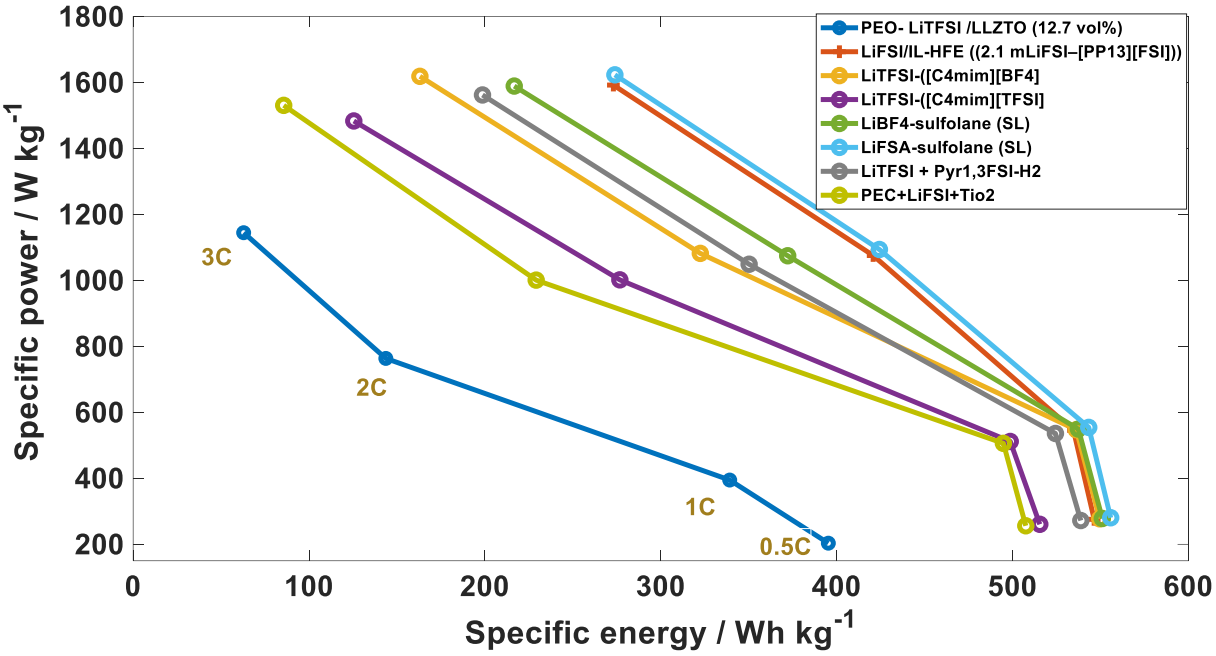

Figure 8. Power density vs specific energy with different cathodic electrolytes for various C-rates for a cell with Li metal as the anode, hybrid SE based on LLZTO as the solid separator, and NMC811 as cathode materials at cathode thickness of 55 µm and solid separator of 40 µm

- **LiFSI/IL-HFE ((2.1 mLiFSI–[PP13][FSI])) [29]**
  - Addition of HFE to the pure ILs (2.1 mLiFSI–[PP13] [FSI]) decreases the viscosity of the electrolytes and enhances the ionic conductivity and its ability to wet the separator surface
  - Excellent electrochemical performance in lithium metal batteries up to 5.4 V
  - Cycling lifespan up to 800
  - Introducing HFE decreases the cost of the pure ionic liquid electrolyte
  - Non-Flammable

- **LiFSA-sulfolane (SL) [33]**
  - Sulfones have high oxidative stability
  - Such electrolytes are expected to be suitable for the development of high-voltage and high-energy-density batteries
  - Li-metal cycling Coulombic efficiency is increased to 98.2% and remains stable for over 150 cycles
  - Effectively suppressing the concentration polarization in a lithium battery

Table 8: Chemistry of the based cell with SE cathodic electrolyte and best and promising HCE as cathodic electrolyte

	Anode	Separator	Cathode
Base electrolyte	*Li*	*hybrid SE based on LLZTO*	*NMC811 & hybrid SE based on LLZTO*
Best HCE			*NMC811 & LiFSA-sulfolane (SL)*
Promising HCE			*NMC811 & LiFSI-IL-HFE*

The performance of the battery with the base cathodic electrolyte, the best-identified cathodic electrolyte, and the most promising one is compared in the following. This comparison uses the same materials for the anode, i.e., lithium metal, NMC811 as active

materials, and electrolyte in the separator layer, namely hybrid SE based on LLZTO (PEO-LiTFSI/LLZTO (12.7 vol%)). The only difference among them is the applied electrolyte in the cathode electrode. We applied electrolyte characteristics for the modelling, such as the lithium transfer number, ionic conductivity, and electrolyte diffusion coefficient based on available experimental data in the literature. Since hybrid SE performs well at a temperature of 60°C as we noted in ref [4], we used the Arrhenius relation to take into account the dependence of electrolyte properties on temperature for those parameters which aren't given at this temperature.

In order to determine how the battery would behave if the cathodic electrolyte of the hybrid solid electrolyte was replaced with one of the two highly concentrated electrolytes identified, a comparative analysis of three cells with different current rates is performed. As shown in Figure 9, the cell with hybrid SE in the cathode performs worst among the other cathodic electrolyte, especially at high C-rates, which lowers the areal capacity. This is a result of the poor transport properties of hybrid SE, which raise overpotentials, change the slope of the discharge curve, and drastically cause the voltage drop. However, using a highly concentrated electrolyte as a cathodic electrolyte instead of a hybrid SE based on LLZTO improves the kinetics of electrode reaction at the electrolyte/electrode interfaces due to greater ionic conductivity and higher Li-ion diffusion coefficient, which causes less polarization.

The areal capacity of the battery can improve by around 106% and 328%, when the battery operates at 2C and 3C, respectively, employing HCE as a cathodic electrolyte rather than a hybrid solid electrolyte. Such high discharge rates expect in high power phases for hybrid electric regional aircraft, in which composite cathodic electrolyte containing HCE could perform well in these C-rate ranges. This emphasises the need for composite cathodic electrolytes including highly concentrated or ionic liquids to meet mission demand requirements, a strategy that is also used in current industry developments, to achieve energy-dense and power-capable cells.

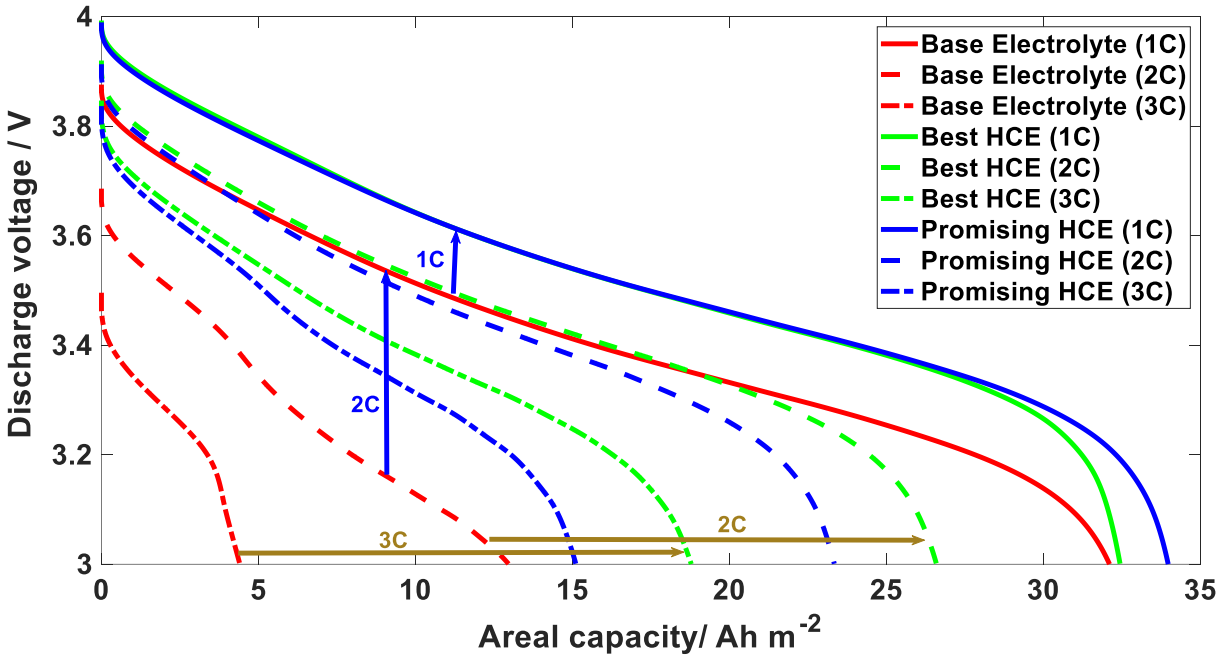

Figure 9. Voltage vs areal capacity with different cathodic electrolytes at different C-rates *for a cell with Li metal as the anode, hybrid SE based on LLZTO as the solid separator, and NMC811 as cathode materials*

3.2. OPTIMIZATION OF CATHODE THICKNESS FOR THE CELL WITH HIGHLY CONCENTRATED ELECTROLYTES AS CATHODIC ELECTROLYTE

So far, it has been shown that using highly concentrated ionic liquid electrolytes in the cathode electrode has a significant influence on the capacity and, consequently, specific energy of the battery cell. Since batteries with thick electrodes could increase the proportion of active materials and therefore specific energy, here we evaluate the effect of the thick electrode on the specific energy to identify the optimum electrode thickness to achieve higher specific energy, particularly at elevated current rates, as illustrated in Figure 10. At 1C, the specific energy increases with increasing electrode thickness up to a critical threshold, as indicated in the figure, but beyond this critical thickness, the specific energy will decrease. This is due to a limitation of mass transfer imposed by a longer diffusion path at a thicker cathode. Additionally, the best cathodic electrolyte has a specific energy of 479 Wh kg^{-1} and 428 Wh kg^{-1} at C-rates of 2C and 3C, respectively. These values are roughly 62% and 190% better than for the cell with hybrid SE based on LLZTO as the cathodic electrolyte. As shown in the figure, when the base electrolyte operates at a higher C-rate, a maximum power density at the cell level can be reached, but with very limited specific energy due to its poor ionic conductivity and tortuosity factor, which results in lower transport properties. Therefore, to address the balance of the battery power and energy density required for aircraft use, it is preferable to use HCE cathodic electrolytes rather than hybrid solid electrolytes, as mentioned before.

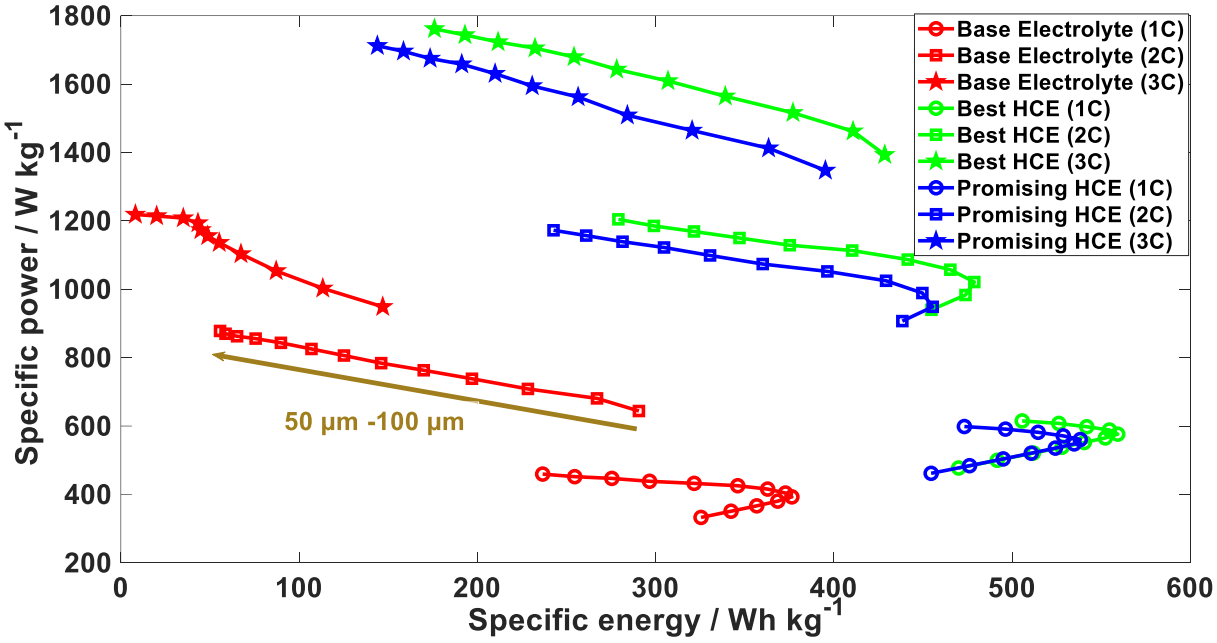

Figure 10. Power density vs specific energy for the various cathodic electrolyte at different electrode thicknesses for a cell with Li metal as the anode, hybrid SE based on LLZTO as the solid separator, and NMC811 as the cathode

In summary using highly concentrated liquid-ionic electrolytes results in:

- Power capability: GED at higher C-rates largely improved:
  - @ 2C: +62%
  - @ 3C: 190%
- High GED & power capability achievable:

- 613 Wh kg^{-1} @ 0.1
- 560 Wh kg^{-1} @ 1C
- 479 Wh kg^{-1} @ 2C
- 428 Wh kg^{-1} @ 3C

As described in Table 9, employing highly concentrated electrolytes leads to improving GED of the battery, especially at a higher C-rate. This makes it possible to achieve high energy and power capacities and is one of the possible options for energy-power-balanced applications.

Table 9: GED of highly concentrated electrolytes as cathodic electrolytes at different C-rates

0.1C			
	Anode	***Cathode***	***GED (cell level)***
Best HCE	*Li*	*NMC811 & LiFSA-sulfolane (SL)*	*613*
Promising HCE		*NMC811 & LiFSI-IL-HFE*	*601*
1C			
	Anode	***Cathode***	***GED (cell level)***
Best HCE	*Li*	*NMC811 & LiFSA-sulfolane (SL)*	*560*
Promising HCE		*NMC811 & LiFSI-IL-HFE*	*540*
2C			
	Anode	***Cathode***	***GED (cell level)***
Best HCE	*Li*	*NMC811 & LiFSA-sulfolane (SL)*	*479*
Promising HCE		*NMC811 & LiFSI-IL-HFE*	*455*
3C			
	Anode	***Cathode***	***GED (cell level)***
Best HCE	*Li*	*NMC811 & LiFSA-sulfolane (SL)*	*428*
Promising HCE		*NMC811 & LiFSI-IL-HFE*	*395*

4. MODELLING BATTERY UNDER DYNAMIC LOAD OF AIRCRAFT

4.1. BATTERY PERFORMANCE UNDER DYNAMIC BATTERY POWER DEMAND FOR REG-CON AIRCRAFT

So far, battery performance for various cathodic electrolytes under a constant current rate was assesed. To examine how these types of electrolytes react under dynamic loading, we apply the battery current demand during the mission for a regional hybrid aircraft. Here,

we used the mission profile of the REG-CON (Regional-Conservative) configuration[1] that Bauhaus Luftfahrt (BHL) provided to include the necessary battery power at different stages of the flight, as shown in Figure 11. In this mission profile, a fully electric operation is used during the taxi-out and taxi-in phases, and the batteries' load is reduced throughout the descent phase to give the necessary power for taxi-in. Additionally, batteries provide electric power for the aircraft's non-propulsive subsystems in all flight phases.

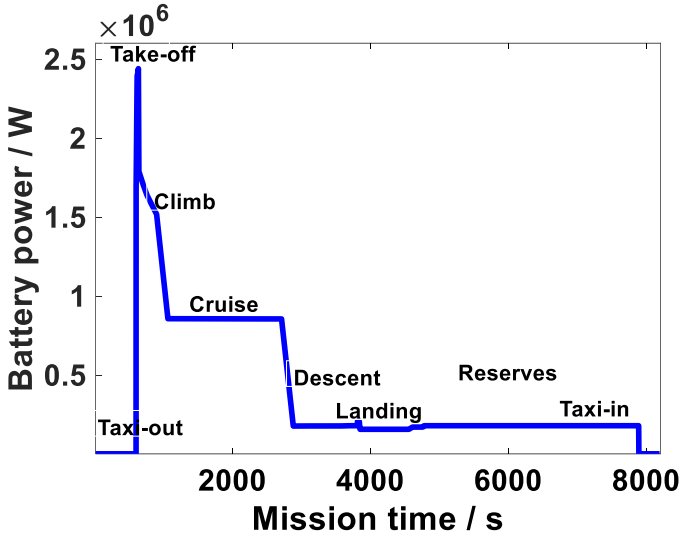

Figure 11. Power demand of battery at different mission stages for REG-CON aircraft

Figure 12 shows the battery performance under transient power demand for REG-CON hybrid aircraft. As it can be seen, the voltage of ASSB with solid electrolyte within the cathode lowers dramatically and cannot fulfil the mission's requirements. This may be caused by the poor ionic conductivity of hybrid SE in the cathode, which results in severe mass transport limitations at higher C rates. However, the battery with HCE cathodic electrolyte performs remarkably better than ASSB. Because HCE has better transport properties than the base electrolyte, this leads to shorter effective ion transport paths and significantly enhances battery performance. Even though under C-rate changes the battery with HCE cathodic electrolyte performs noticeably better than base electrolytes, the mission demand in the reserved phase still cannot be satisfied by these two electrolytes.

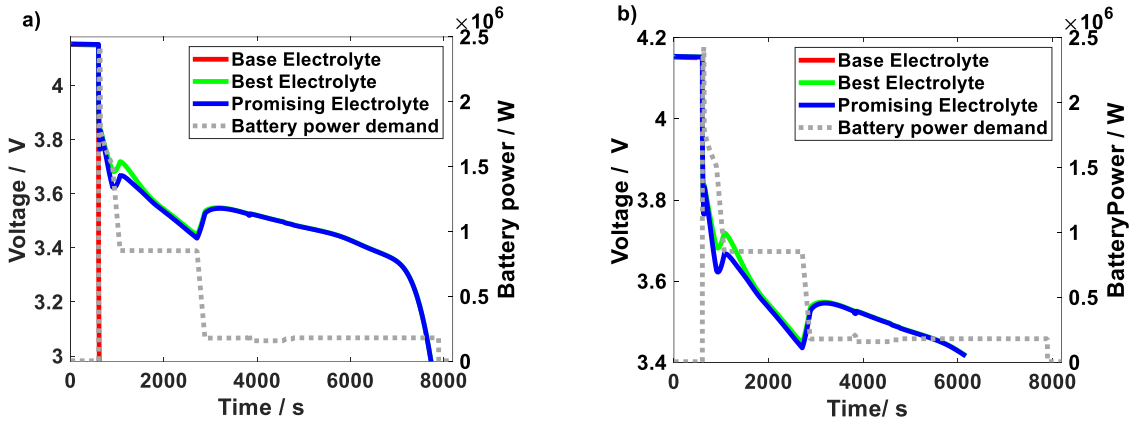

Figure 12. Battery performance under dynamic battery power demand for REG-CON aircraft with various cathodic electrolytes for a battery cell with Li metal as the anode, hybrid SE based on LLZTO as the solid separator, and NMC811 as the cathode at, a) DOD of 100%, b) DOD 80%

[1] https://www.imothep-project.eu/project-scope-20

4.2. HEAT GENERATION OF BATTERY UNDER DYNAMIC DEMAND

Even if highly concentrated liquid and ionic electrolytes and solid electrolytes are inflammable and thermally stable in contact with Li metal anode, further research is still needed to completely understand how energy-dense cathode materials affect cell safety. Therefore, it is essential to look into the battery's heat generation, particularly during different flight missions. To this end, after modelling the battery under dynamic power demand, a simple model to predict heat generation, $\dot{Q}_{tot}$, at various flight phases was implemented. Reversible heat, $\dot{Q}_r$, and irreversible heat, $\dot{Q}_{irr}$, are two types of internal heat produced within the battery during its operation, which can be calculated using Equation 1.

$$\dot{Q}_{tot} = \dot{Q}_{irr} + \dot{Q}_r \qquad \text{Total heating} \tag{6}$$

Joule heating causes the first term of heat generation, and entropy changes, ΔS, cause the second term. The ohmic overpotential, and reaction and concentration polarization overpotentials, which causes the irreversible heat generation rate, can be calculated using the formula shown below [36,37]:

$$\dot{Q}_{irr} = (U_0 - V)i \qquad \text{Joule heating} \tag{7}$$

$$\dot{Q}_r = -T\Delta S\frac{i}{nF} \qquad \text{Reversible heating during discharge} \tag{8}$$

where i is current and n is the number of electrons transferred in the electrochemical reaction. The discharge reaction for a cathode is represented by the entropy change in a full cell, which typically corresponds to a reduction reaction [38]. The structural changes of the active materials during operation are connected to the entropy variation ΔS. Depending on the state of charge (SOC) and the current sign, the corresponding energy changes could cause heat generation or heat consumption [39]. Thus, the reversible heat is proportional to operating current and entropy changes and it can be generated or consumed during reversible intercalation and deintercalation of lithium during charging and discharging. According to Zhao's work [40], we applied the dependency of entropy changes for NMC materials versus SOC, as illustrated in Figure 13 to predict the reversible heat. By differentiating overvoltages from open circuit voltage, the Joule heating can be estimated, as noted above.

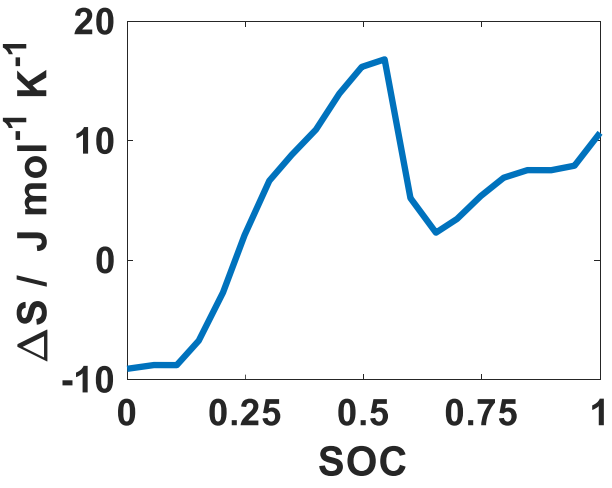

Figure 13. Entropy change of NMC versus SOC [40]

Figure 14 shows the percentage of heat released at different depths of discharge (DOD) and various current rates for the cell with different cathodic electrolytes. As shown by the equations above, heat production resulting from entropy change and Joule heating is proportional to discharge current. An increase in C-rate increases local electrochemical reactions in the electrode, which increases the rate of heat generation. The base cell with hybrid solid as cathodic electrolyte suffers from severe mass transport constraints at high C-rates, which causes a dramatic drop in the cell voltage and heat generation. At 3C, up to 25% of electricity is converted to heat, as shown in Figure 14-a. This is because of the low ionic conductivity of semi-solid electrolytes in comparison to liquid electrolytes, which results in high Joule heating and heat loss. In contrast, utilising HCE results in superior mass transportation at high C-rates of 3C, the maximum required current rates of battery for regional aircraft in this study, where 12% of power is converted to heat. Further, there is no significant difference in terms of heat generation using the best and most promising cathodic electrolyte under constant load.

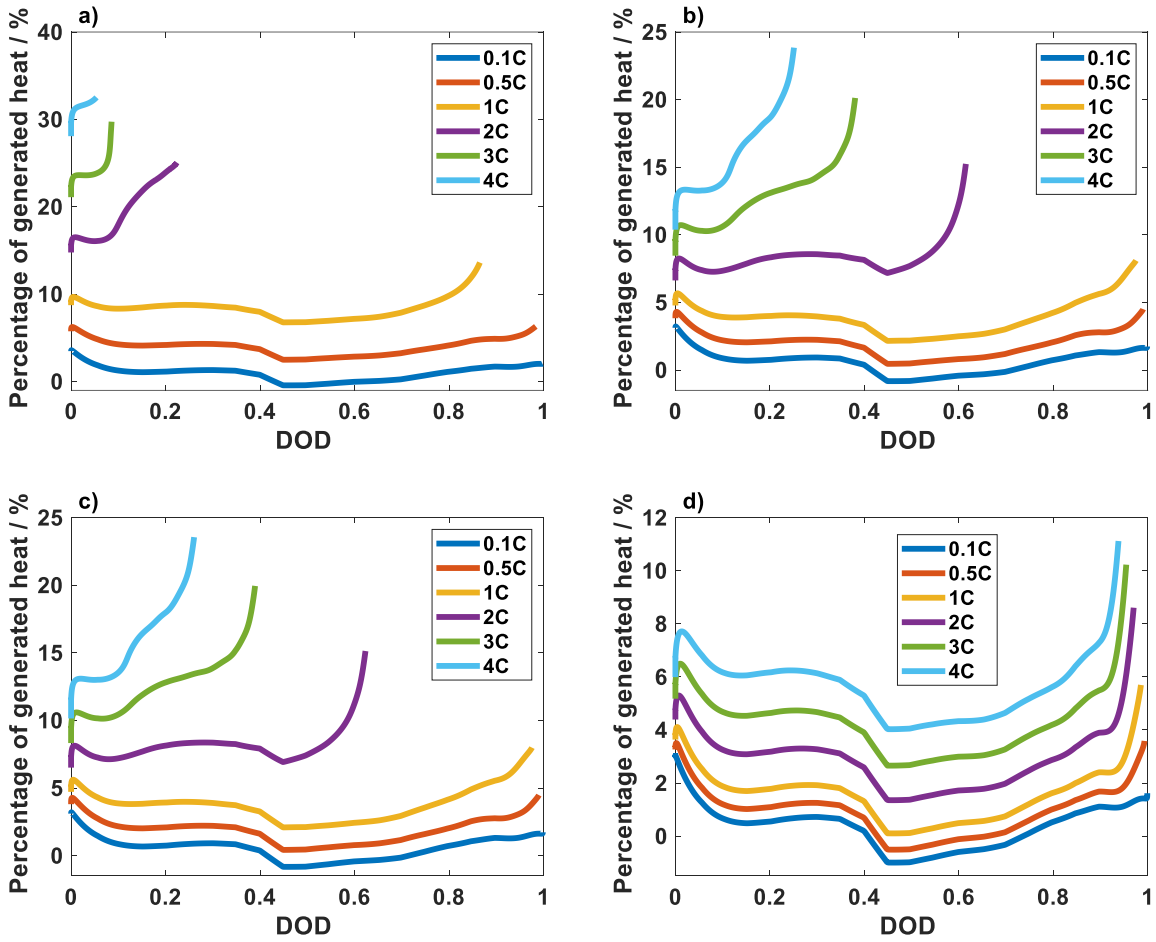

Figure 14. Percentage of heat release at different discharge rates and DOD for a battery cell with Li metal as the anode, hybrid SE based on LLZTO as the solid separator, and NMC811 as the cathode, and a) base cathodic electrolyte, b) best cathodic electrolyte, c) promising cathodic electrolyte, d) employing liquid electrolyte as separator and cathodic electrolyte

Liquid electrolyte was also employed in the separator and as the cathodic electrolyte, and then we investigated the heat generation in the battery. As shown in Figure 14-d, approximately 4.5% of the power is converted to heat at 3C at different DOD, which is within the range measured by AIT for ultra-high-power cells.

Table 10: Heat release of a commercial ultra-high power cell measured with the battery cell calorimeter at AIT

AIT UHP cell measurements		283 K	298 K	313 K
Discharge, 3C	Constant current	7.57%	5.09%	4.17%
Charge, 2C	Constant current only	5.15%	3.28%	2.70%
Charge, 4C	Constant current only	7.61%	5.54%	4.66%

Following, the amount of heat generation for the battery cell was examined with the best cathodic electrolyte, LiFSI-IL-HFE, under dynamic power load. As illustrated in Figure 15, it is clear that the battery current is greater during the take-off phase than during the cruise phase. The aircraft has a relatively low power requirement throughout the climb, cruise, and descent phases, and the current's magnitude also sharply reduces in these phases of the mission. At a higher discharge current, more heat will be generated, and the irreversible heat is dominant at these C-rate ranges.

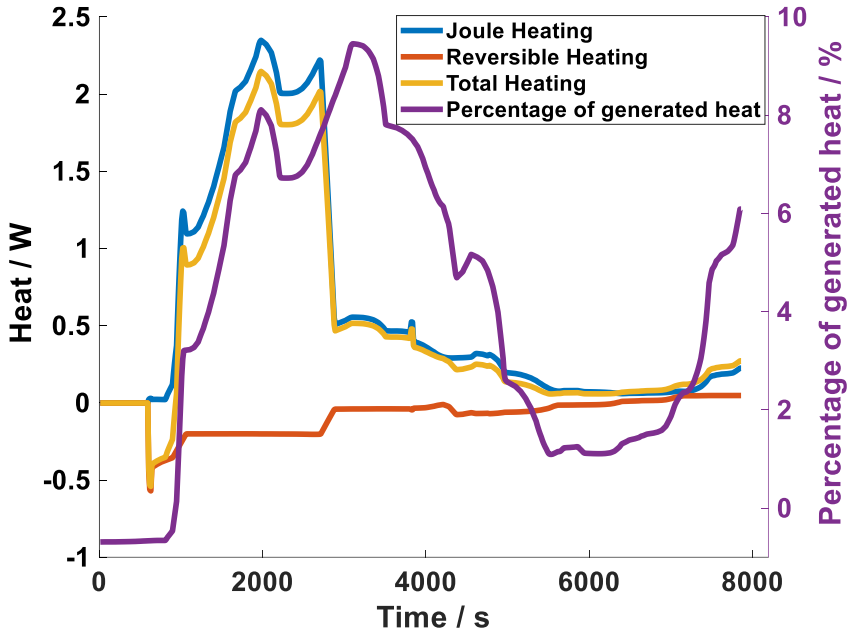

Figure 15. Heat generation inside battery cell with respect to mission demand for a cell with Li metal as the anode, hybrid SE based on LLZTO as the solid separator, and NMC811 & LiFSI-IL-HFE as cathodic electrolyte

The findings of this section help battery engineers and researchers to better understand the thermal behaviour of ASSB with HCE as a cathodic electrolyte and to make much more precise predictions about the heat generation in the battery. This outcome is also useful for optimising cell design and operation, building efficient thermal management systems, and offering precise battery management systems for various battery applications. However, there is still a need for the development of battery cell technologies for aircraft applications that are cost-effective, simultaneously have an appropriate cycle life, and have high safety while also having an ultra-high energy density and sufficient power capacity, which can operate in an aeronautic environment.

5. CONCLUSIONS AND PROSPECTS

In summary, physics-based modelling of the battery was used to predict the optimal design parameters of ASSB to attain a higher gravimetric energy density for aerial applications, which could help experimental research to improve cell design with more time and cost-efficiency. The following conclusions can be drawn from the physics-based modelling of the battery.

- ASSB based on 12.7 vol% of LLZTO is the best option based on present manufacturing constraints.
- The optimal proposed design for a particular application does not perform well for all applications.
- Capacity and GED at higher discharge rates largely improved using highly concentrated ILs inside the cathode electrode and as a result, high energy and power capabilities are possible using such type of cathodic electrolyte.
- Employing highly concentrated ILs as cathodic electrolytes causes an improvement in GED of battery cells by nearly 62% and 190% compared to the cell using hybrid SE based on LLZTO as the cathodic electrolyte at 2C and 3C, respectively.
- Employing HCE as a cathodic electrolyte-type electrolyte could significantly improve battery performance under dynamic mission load.
- Although the identified electrolyte considerably enhances battery capacity, aeronautic battery cells must be optimised to accomplish aviation's aim, which includes lowering weight penalties, improving battery safety issues, allowing deeper discharge with still high power output, and permitting continuous quick charge and discharge to shorten time on the ground.

6. MAIN COLLABORATION AND DISSEMINATION ACTIVITIES

The dissemination activities of WP4.2 are summarised in the following:

- KIT in cooperation with AIT is under preparation of the following paper:
  - Perspective study of using highly concentrated electrolytes for aeronautic battery
- KIT in cooperation with AIT presented the result of the IMOTHEP project at the 72nd Annual Meeting of the International Society of Electrochemistry in Jeju Island, Korea, and 24^{2nd} ECS Meeting, in Atlanta, GA.
- The collaborative paper between KIT and AIT based on the IMOTHEP results is published in the journal of the Electrochemical Society. https://iopscience.iop.org/article/10.1149/1945-7111/ac653b/meta
- In September 2021, Somayeh Toghyani (KIT) visited AIT for one month within a research stay funded by the Karlsruhe House of Young Scientists (KHYS) within the framework of Connecting Young Scientists (ConYS) (complementary to IMOTHEP) to deepen the understanding of the interlink between experimental and modelling activities. During this stay, the following activities were conducted:

- Design and prepare slurries of NMC811 with different NMC loadings:80wt%, 85wt%, and 90wt%.
- Coating and calendaring of NMC811 cathode sheets.
- Design and preparation of PEO-based hybrid solid electrolyte with LLZO as active filler.
- Assembly of a series of all-solid-state lithium-ion battery coin-cells for electrochemical characterization at KIT.

7. REFERENCES

[1] H2020 IMOTHEP. https://www.imothep-project.eu/.

[2] V. Viswanathan, A.H. Epstein, Y.M. Chiang, E. Takeuchi, M. Bradley, J. Langford, M. Winter, The challenges and opportunities of battery-powered flight, Nature. 601 (2022) 519–525. https://doi.org/10.1038/s41586-021-04139-1.

[3] M. Weiss, F.J. Simon, M.R. Busche, T. Nakamura, D. Schröder, F.H. Richter, J. Janek, From Liquid- to Solid-State Batteries: Ion Transfer Kinetics of Heteroionic Interfaces, Electrochem. Energy Rev. 3 (2020) 221–238. https://doi.org/10.1007/s41918-020-00062-7.

[4] S. Toghyani, F. Baakes, N. Zhang, H. Kuehnelt, W. Cistjakov, U. Krewer, Model-Based Design of High Energy All-Solid-State Li Batteries with Hybrid Electrolytes, J. Electrochem. Soc. (2022). https://doi.org/10.1149/1945-7111/ac653b.

[5] J. Schnell, T. Günther, T. Knoche, C. Vieider, L. Köhler, A. Just, M. Keller, S. Passerini, G. Reinhart, All-solid-state lithium-ion and lithium metal batteries – paving the way to large-scale production, J. Power Sources. 382 (2018) 160–175. https://doi.org/10.1016/j.jpowsour.2018.02.062.

[6] U. Krewer, F. Röder, E. Harinath, R.D. Braatz, B. Bedürftig, R. Findeisen, Review—Dynamic Models of Li-Ion Batteries for Diagnosis and Operation: A Review and Perspective, J. Electrochem. Soc. 165 (2018) A3656–A3673. https://doi.org/10.1149/2.1061814jes.

[7] A. Jokar, B. Rajabloo, M. Désilets, M. Lacroix, Review of simplified Pseudo-two-Dimensional models of lithium-ion batteries, J. Power Sources. 327 (2016) 44–55. https://doi.org/10.1016/j.jpowsour.2016.07.036.

[8] L. Zhu, P. Zhu, Q. Fang, M. Jing, X. Shen, L. Yang, A novel solid PEO/LLTO-nanowires polymer composite electrolyte for solid-state lithium-ion battery, Electrochim. Acta. 292 (2018) 718–726. https://doi.org/10.1016/j.electacta.2018.10.005.

[9] L. Zhu, P. Zhu, S. Yao, X. Shen, F. Tu, High-performance solid PEO/PPC/LLTO-nanowires polymer composite electrolyte for solid-state lithium battery, Int. J. Energy Res. 43 (2019) 4854–4866. https://doi.org/10.1002/er.4638.

[10] J. Zhang, N. Zhao, M. Zhang, Y. Li, P.K. Chu, X. Guo, Z. Di, X. Wang, H. Li, Flexible and ion-conducting membrane electrolytes for solid-state lithium batteries: Dispersion of garnet nanoparticles in insulating polyethylene oxide, Nano Energy. 28 (2016) 447–454. https://doi.org/10.1016/j.nanoen.2016.09.002.

[11] F. Ma, Z. Zhang, W. Yan, X. Ma, D. Sun, Y. Jin, X. Chen, K. He, Solid Polymer Electrolyte Based on Polymerized Ionic Liquid for High Performance All-Solid-State Lithium-Ion Batteries, ACS Sustain. Chem. Eng. 7 (2019) 4675–4683. https://doi.org/10.1021/acssuschemeng.8b04076.

[12] G. Piana, F. Bella, F. Geobaldo, G. Meligrana, C. Gerbaldi, PEO/LAGP hybrid solid polymer electrolytes for ambient temperature lithium batteries by solvent-free, "one pot" preparation, J. Energy Storage. 26 (2019) 100947. https://doi.org/10.1016/j.est.2019.100947.

[13] Y. Meesala, Y.-K. Liao, A. Jena, N.-H. Yang, W.K. Pang, S.-F. Hu, H. Chang, C.-E. Liu, S.-C. Liao, J.-M. Chen, An efficient multi-doping strategy to enhance Li-ion conductivity in the garnet-type solid electrolyte Li 7 La 3 Zr 2 O 12, J. Mater. Chem. A. 7 (2019) 8589–8601.

[14] Z. Zhang, Y. Shao, B. Lotsch, Y.S. Hu, H. Li, J. Janek, L.F. Nazar, C.W. Nan, J. Maier,

M. Armand, L. Chen, New horizons for inorganic solid state ion conductors, Energy Environ. Sci. 11 (2018) 1945–1976. https://doi.org/10.1039/c8ee01053f.
[15] W. Zhao, J. Yi, P. He, H. Zhou, Solid-State Electrolytes for Lithium-Ion Batteries: Fundamentals, Challenges and Perspectives, Springer Singapore, 2019. https://doi.org/10.1007/s41918-019-00048-0.
[16] K. Waetzig, A. Rost, C. Heubner, M. Coeler, K. Nikolowski, M. Wolter, J. Schilm, Synthesis and sintering of Li1.3Al0.3Ti1.7(PO4)3 (LATP) electrolyte for ceramics with improved Li+ conductivity, J. Alloys Compd. 818 (2020) 153237. https://doi.org/10.1016/j.jallcom.2019.153237.
[17] S. Wang, Y. Ding, G. Zhou, G. Yu, A. Manthiram, Durability of the Li1+ x Ti2–x Al x (PO4) 3 Solid Electrolyte in Lithium–Sulfur Batteries, ACS Energy Lett. 1 (2016) 1080–1085.
[18] L. Fan, S. Wei, S. Li, Q. Li, Y. Lu, Recent Progress of the Solid-State Electrolytes for High-Energy Metal-Based Batteries, Adv. Energy Mater. 8 (2018) 1–31. https://doi.org/10.1002/aenm.201702657.
[19] J. Sturm, S. Ludwig, J. Zwirner, C. Ramirez-Garcia, B. Heinrich, M.F. Horsche, A. Jossen, Suitability of physicochemical models for embedded systems regarding a nickel-rich, silicon-graphite lithium-ion battery, J. Power Sources. 436 (2019) 226834.
[20] N. Lin, X. Xie, R. Schenkendorf, U. Krewer, Efficient Global Sensitivity Analysis of 3D Multiphysics Model for Li-Ion Batteries, J. Electrochem. Soc. 165 (2018) A1169–A1183. https://doi.org/10.1149/2.1301805jes.
[21] D. Witt, D. Wilde, F. Baakes, F. Belkhir, F. Röder, U. Krewer, Myth and Reality of a Universal Lithium-Ion Battery Electrode Design Optimum: A Perspective and Case Study, Energy Technol. (2021). https://doi.org/10.1002/ente.202000989.
[22] X. Ren, L. Zou, X. Cao, M.H. Engelhard, W. Liu, S.D. Burton, H. Lee, C. Niu, B.E. Matthews, Z. Zhu, C. Wang, B.W. Arey, J. Xiao, J. Liu, J.G. Zhang, W. Xu, Enabling High-Voltage Lithium-Metal Batteries under Practical Conditions, Joule. 3 (2019) 1662–1676. https://doi.org/10.1016/j.joule.2019.05.006.
[23] H. Löbberding, S. Wessel, C. Offermanns, M. Kehrer, J. Rother, H. Heimes, A. Kampker, From cell to battery system in BEVs: Analysis of system packing efficiency and cell types, World Electr. Veh. J. 11 (2020) 1–15. https://doi.org/10.3390/wevj11040077.
[24] I. Sobol, Sensitivity estimates for nonlinear mathematical models, Mater, (1990).
[25] V. Triantafyllidiis, W.W. Xing, P.K. Leung, A. Rodchanarowan, A.A. Shah, Probabilistic sensitivity analysis for multivariate model outputs with applications to Li-ion batteries, J. Phys. Conf. Ser. 1039 (2018). https://doi.org/10.1088/1742-6596/1039/1/012020.
[26] G. Merei, C. Berger, D.U. Sauer, Optimization of an off-grid hybrid PV-Wind-Diesel system with different battery technologies using genetic algorithm, Sol. Energy. 97 (2013) 460–473. https://doi.org/10.1016/j.solener.2013.08.016.
[27] H.Q. Pham, H.Y. Lee, E.H. Hwang, Y.G. Kwon, S.W. Song, Non-flammable organic liquid electrolyte for high-safety and high-energy density Li-ion batteries, J. Power Sources. 404 (2018) 13–19. https://doi.org/10.1016/j.jpowsour.2018.09.075.
[28] Z. Wang, Y. Sun, Y. Mao, F. Zhang, L. Zheng, D. Fu, Y. Shen, J. Hu, H. Dong, J. Xu, X. Wu, Highly concentrated dual-anion electrolyte for non-flammable high-voltage Li-metal batteries, Energy Storage Mater. 30 (2020) 228–237. https://doi.org/10.1016/j.ensm.2020.05.020.
[29] Z. Wang, F. Zhang, Y. Sun, L. Zheng, Y. Shen, D. Fu, W. Li, A. Pan, L. Wang, J. Xu, J. Hu, X. Wu, Intrinsically Nonflammable Ionic Liquid-Based Localized Highly Concentrated Electrolytes Enable High-Performance Li-Metal Batteries, Adv. Energy Mater. 11 (2021) 1–8. https://doi.org/10.1002/aenm.202003752.
[30] J. Mao, W. Tiedemann, J. Newman, Simulation of temperature rise in Li-ion cells at very high currents, J. Power Sources. 271 (2014) 444–454.
[31] J. Tong, S. Wu, N. von Solms, X. Liang, F. Huo, Q. Zhou, H. He, S. Zhang, The Effect of Concentration of Lithium Salt on the Structural and Transport Properties of Ionic Liquid-Based Electrolytes, Front. Chem. 7 (2020) 1–10.

https://doi.org/10.3389/fchem.2019.00945.
[32] J. Tong, X. Xiao, X. Liang, N. Von Solms, F. Huo, H. He, S. Zhang, Insights into the solvation and dynamic behaviors of a lithium salt in organic- and ionic liquid-based electrolytes, Phys. Chem. Chem. Phys. 21 (2019) 19216–19225. https://doi.org/10.1039/c9cp01848d.
[33] K. Dokko, D. Watanabe, Y. Ugata, M.L. Thomas, S. Tsuzuki, W. Shinoda, K. Hashimoto, K. Ueno, Y. Umebayashi, M. Watanabe, Direct Evidence for Li Ion Hopping Conduction in Highly Concentrated Sulfolane-Based Liquid Electrolytes, J. Phys. Chem. B. 122 (2018) 10736–10745. https://doi.org/10.1021/acs.jpcb.8b09439.
[34] H. Zhang, W. Qu, N. Chen, Y. Huang, L. Li, F. Wu, R. Chen, Ionic liquid electrolyte with highly concentrated LiTFSI for lithium metal batteries, Electrochim. Acta. 285 (2018) 78–85. https://doi.org/10.1016/j.electacta.2018.07.231.
[35] Y. Tominaga, K. Yamazaki, Fast Li-ion conduction in poly(ethylene carbonate)-based electrolytes and composites filled with TiO2 nanoparticles, Chem. Commun. 50 (2014) 4448–4450. https://doi.org/10.1039/c3cc49588d.
[36] K. Murashko, A. V Mityakov, J. Jokiniemi, Determination of the entropy change profile of a cylindrical lithium-ion battery by heat flux measurements, (2016). https://doi.org/10.1016/j.jpowsour.2016.08.130.
[37] L.B. Diaz, A. Hales, M.W. Marzook, Y. Patel, G. Offer, Measuring irreversible heat generation in lithium-ion batteries: an experimental methodology, J. Electrochem. Soc. 169 (2022) 30523.
[38] V. V Viswanathan, D. Choi, D. Wang, W. Xu, S. Towne, R.E. Williford, J. Zhang, J. Liu, Z. Yang, Effect of entropy change of lithium intercalation in cathodes and anodes on Li-ion battery thermal management, J. Power Sources. 195 (2010) 3720–3729. https://doi.org/10.1016/j.jpowsour.2009.11.103.
[39] N. Damay, C. Forgez, M. Bichat, G. Friedrich, N. Damay, C. Forgez, M. Bichat, G. Friedrich, A method for the fast estimation of a battery entropy-variation high-resolution curve – Application on a commercial LiFePO4 / graphite cell To cite this version : HAL Id : hal-02007386, (2019).
[40] W. Zhao, M. Rohde, I.U. Mohsin, C. Ziebert, Heat Generation in NMC622 Coin Cells during Electrochemical Cycling : Separation of Reversible and Irreversible Heat E ff ects, (2020).